communications medicine

A Nature Portfolio journal

Article

https://doi.org/10.1038/s43856-025-00911-w

Natural killer cells adopt an activated and decidual-like phenotype after autologous hematopoietic stem cell transplantation in children with cancer

A list of authors and their affiliations appears at the end of the paper

Abstract

Background Natural killer (NK) cells are among the first immune cell populations to recover after autologous hematopoietic stem cell transplantation (autoHSCT), yet their dynamic function in pediatric patients remains understudied. Investigating NK cell recovery could improve understanding of post-autoHSCT immune reconstitution and optimize clinical outcomes.

Methods We characterized NK cells in 13 children (male: 8; female: 5; age range: 3–11 years) with various tumors before and up to 6 months after autoHSCT. Multiparametric flow cytometry analyses and plasma cytokine level determinations were performed. In vitro experiments, including single-cell RNA sequencing, were conducted to elucidate post-autoHSCT changes in the NK cell repertoire using 8 adult healthy donors (male: 5; female: 3; age range: 25–62 years).

Results Key findings highlight a transient decidual-like NK cell phenotype emerging early post-transplant. These cells are immature and activated, with increased inhibitory receptor expression and diminished activating receptor levels. This activated and decidual-like phenotype is characterized by elevated expression of CD56, CD9, CD49a, CD151, CD38, HLA-DR, and CD55. Plasma levels of several cytokines are associated with the observed changes in NK cells' phenotype. In addition, in vitro experiments recapitulate the alterations observed in NK cells shortly after autoHSCT. Specifically, results demonstrate that the combination of IL-15 and TGF-β induces this distinctive phenotype on NK cells after autoHSCT. Finally, we observe a positive correlation between relapse and the percentage of $CD56^{dim}$ NK cells shortly after autoHSCT in our cohort of pediatric patients.

Conclusions Altogether, our findings provide valuable insights into the physiopathology of NK cells during immune system reconstitution after autoHSCT and can potentially help in the management of cancer in children.

Plain language summary

Autologous hematopoietic stem cell transplantation (autoHSCT) is a common cancer treatment that transplants a patient's own blood stem cells. However, the autoHSCT function in pediatric patients is not fully understood. Here, we find that natural killer (NK) cells, which help fight cancer, change significantly right after autoHSCT in children with cancer. NK cells temporarily express cell membrane proteins similar to those found in pregnancy and become more active. These NK cells show membrane proteins called receptors that modify their function: activating or inhibiting them. Their inhibitory receptors (off switches) increase, while activating receptors (on switches) decrease. These modifications are linked to certain molecules in the blood called cytokines. Lab tests show that two molecules, IL-15 and TGF-β, together cause these alterations in NK cells. Understanding these changes may help improve treatment and care for children after autoHSCT treatment.

Autologous hematopoietic stem cell transplantation (autoHSCT) is a widespread procedure used to treat many different types of cancer, including hematological tumors in adults and solid tumors in children. It is a relatively common therapeutic tool to combat not only hematological malignancies, such as multiple myeloma (MM) or non-Hodgkin lymphoma (NHL), but also for some pediatric solid tumors, such as neuroblastoma, and might be a salvage option for other tumors like lymphomas and sarcomas[1–3].

Early immune reconstitution following autoHSCT is associated with a better outcome in a variety of cancers[4–6]. Day 15 absolute lymphocyte count (ALC-15) of ≥500 cells/μl after autoHSCT is an independent prognostic indicator in MM and NHL patients. Natural killer (NK) cells are a relevant lymphocyte subset in ALC-15 that affects the outcome following autoHSCT, as they are the first lymphocyte subset reaching normal circulating levels after HSCT[5,7,8].

e-mail: francisco.borregorabasco@bio-bizkaia.eus

NK cells can directly kill target cells through different mechanisms, and they have a central role in the defense against virus-infected and cancer cells[9]. Human circulating NK cells have been classified into two major subsets with different functionalities, depending on the expression of CD56 and CD16: $CD56^{bright}CD16^{low/-}$ ($CD56^{bright}$) and $CD56^{dim}CD16+$ ($CD56^{dim}$). $CD56^{bright}$ NK cells produce large amounts of immunomodulatory cytokines and chemokines but have low cytotoxicity unless they are activated by cytokines. On the other hand, $CD56^{dim}$ NK cells are more cytotoxic but produce lower amounts of cytokines[10,11]. NK cells express activating and inhibitory receptors whose integrated signals will determine their response[12]. In this manner, they do not get activated when they recognize autologous determinants such as class I human leukocyte antigens (HLA-I) through inhibitory killer immunoglobulin-like receptors (KIRs) and CD94/NKG2A receptor. On the other hand, NK cells are activated when they interact with virus-infected or cancer cells, either by the direct detection of upregulated stress-induced self-molecules or via antibody-dependent cell-mediated cytotoxicity[13,14]. Given the potent anti-tumor effect of NK cells and their early recovery after autoHSCT, studying their biology and reconstitution in this setting is of utmost interest. Studies are scarce, and they are mostly focused on adult patients. They show that following autoHSCT, and shortly after leukocyte recovery, there is a redistribution of NK cell subsets. For example, in patients with MM and lymphoma, it has been described that there is an increased frequency of immature $CD56^{bright}NKG2A+$ NK cells, expressing high levels of KIRs and CD57, early after transplant[15]. Another MM study showed a similar redistribution of NK cell populations characterized by a high proliferative rate and an increase in the frequency of both $CD56^{bright}$ NK cells as well as the most immature population within the $CD56^{dim}$ NK subset (CD57-NKG2A+)[16]. In general, NK cell function recovers early after autoHSCT[15,16], and transcriptomic analyses have revealed profound changes related, among others, to cell cycle, DNA replication, and the mevalonate pathway[17]. Interestingly, following autoHSCT in MM patients, there is an expansion of a CD9+ decidual-like NK cell subset that is characterized by high granzyme B and perforin expression levels and exhibits some altered effector functions (degranulation and MIP1β production)[17]. Nevertheless, the factors responsible for this CD9+ NK cell subset expansion are not known.

Specific gene signatures have been associated with survival in cancer patients[18]. In addition, the number of NK cells and the frequency of several subsets are associated with overall and progression-free survival (PFS) in MM and NHL patients following an autoHSCT[8,19]. For example, it has been shown that MM patients with lower frequencies of the mature highly differentiated NKG2A-CD57+ NK cell subset after autoHSCT had a better outcome[16]. Other researchers have found that MM patients in long-term complete response after autoHSCT exhibit a higher frequency of NK cells expressing the inhibitory receptors KIR2DL1 and NKG2A and reduced numbers of NKp46+ NK cells[20]. Interestingly, as in allogeneic HSCT (alloHSCT), there could be a NK cell-mediated graft-versus-tumor (GvT) effect in autoHSCT, that is related to the inhibitory KIR-HLA-I receptor-ligand mismatch and affinity interactions between them[21–25]. Indeed, KIR and HLA-I genotypes have shown to have a significant influence on neuroblastoma patients undergoing autoHSCT and anti-GD2 treatment[22,26].

Despite the advances in adults, in pediatric patients, there is still a substantial need to understand the complexity of the immune system reconstitution after autoHSCT. In this context, an in-depth characterization of the NK cell lymphocyte subset, exploring the biology and physiopathology of NK cells in pediatric patients, would be of great value. In the present study, we have found that following autoHSCT, there are significant changes in the expression of inhibitory and activating receptors, as well as in activation markers, together with a transient expansion of NK cells with a decidual-like phenotype. Furthermore, plasma levels of soluble molecules that are relevant for NK cell differentiation, survival, and function were analyzed. Changes in the levels of interleukin 15 (IL-15) in combination with transforming growth factor beta 1 (TGF-β1 or TGF-β hereafter) may explain the acquisition of the decidual-like phenotype. Also, analyses of maturation markers and KIR expression indicate that NK cell education and maturation are uncoupled processes. Altogether, our findings can be of relevance to understand the biology and physiopathology of NK cells during their reconstitution following autoHSCT and, therefore, help to design better therapies for children with cancer.

Table 1 | Patients' clinical characteristics

		n (%)
Gender	Male	8 (61.5%)
	Female	5 (38.5%)
Cancer type[a]	Neuroblastoma	4 (30.8%)
	Other tumors	9 (69.2%)
Mobilization regimen	G-CSF	13 (100%)
Conditioning regimen	Busulfan-melphalan	4 (30.8%)
	Melphalan	3 (23.1%)
	Thiotepa + cyclophosphamide	2 (15.4%)
	Other	4 (30.8%)
Second HSCT	Yes	5 (38.5%)
	No	8 (61.5%)
Complementary treatment	Radiotherapy	3 (23.1%)
	G-CSF	2 (15.4%)
	G-CSF ± opioids ± antibiotics	5 (38.5%)
	No	3 (23.1%)
Complications after HSCT	Yes	12 (92.3%)
	No	1 (7.7%)
Maintenance regimen	Anti-GD2 + cis-retinoic acid	3 (23.1%)
	Anti-GD2 + rapamycin	1 (7.7%)
	Lenalidomide + bortezomib	1 (7.7%)
	No	8 (61.5%)
Relapse	Yes	6[b] (46.2%)
	No	7 (53.8%)
Dead	Yes	3 (23.1%)
	No	10 (76.9%)
Median (interquartile range)		
Age		4 (3–11)
Infused CD34+ cells ($\times 10^6$ cells/kg)		5.6 (5.3–6.4)

G-CSF granulocyte colony-stimulating factor.
[a]Cancer types are neuroblastoma[b] and other tumors, including: clear cell renal cell carcinoma[b], rhabdoid tumor[b], paraspinal medulloepithelioma, plasmacytoma, Burkitt's lymphoma, embryonal tumor with multilayered rosettes, high-grade neuroepithelial tumor with BCOR (BCL6 corepressor) alteration, acute promyelocytic leukemia, and nephroblastoma.
[b]Patients who have relapsed.

Methods

Patients' characteristics and study design

Blood samples in EDTA-containing tubes from 13 children (male: 8; female: 5; age range: 3–11 years) diagnosed with different cancers and that received autoHSCT were collected for this study at Cruces and Donostia University Hospitals in the Basque Country. Patients' clinical features are described in Table 1. Samples were obtained at five different time points: pre-transplantation (S1), after reaching leukocyte recovery: more than 1000 leukocytes/μl, usually around day 12 after autoHSCT (S2), 30 days after autoHSCT (S3), 100 days after autoHSCT (S4), and 180 days after autoHSCT (S5). Blood samples from 8 adult healthy donors (male: 5; female: 3; age range: 25–62 years) were also collected. Sample collection was carried out through the Basque Biobank for Research (https://www.biobancovasco.bioef.eus), which complies with the quality management, traceability, and biosecurity set out in the Spanish Law 14/2007 of Biomedical Research and

in the Royal Decree 1716/2011. The study was approved by the Basque Ethics Committee for Clinical Research (BIO14/TP/003, PI+CES+INC-BIOEF 2017-03) and the Cruces University Hospital Ethics Committee (E23/78). All adult participants, along with the parents or legal guardians of pediatric patients, provided written and signed informed consent to participate in this study, in accordance with the Declaration of Helsinki.

Sample preparation

Whole blood samples from cancer patients were collected to obtain plasma and PBMCs. For in vitro experiments, PBMCs were isolated from buffy coats and whole blood samples from eight adult healthy donors. Plasma was obtained by centrifugation, while PBMCs were enriched using density gradient centrifugation. The isolated PBMCs were cryopreserved in heat-inactivated fetal bovine serum (FBS) (GE Healthcare HyClone) supplemented with 10% dimethyl sulfoxide (Thermo Scientific) and stored in liquid nitrogen.

Cryopreserved PBMCs were thawed at 37 °C in a water bath and washed twice with RPMI 1640 medium with L-Glutamine (Lonza). After that, cells were incubated for 1 h at 37 °C and 5% CO_2 with 10U DNase (Roche) in R10 medium (RPMI 1640 medium containing GlutaMAX, 10% FBS, and 1% Penicillin-Streptomycin, from Thermo Fisher Scientific). Following incubation, the cells were washed once, resuspended in NK cell medium (RPMI 1640 medium with GlutaMAX, 10% FBS, 1% P-S, 1% MEM Non-Essential Amino Acids Solution, and 1% Sodium Pyruvate, from Thermo Fisher Scientific), filtered through 70 µm cell strainers, and counted. The processed PBMCs were then used in flow cytometry or in vitro experiments.

NK cell absolute number quantification

Whole blood samples were used to quantify the absolute number of NK cells. NK cells were identified as CD45+, CD3−, CD56+ and/or CD16+ lymphocytes using the following clinical-grade fluorochrome-conjugated monoclonal antibodies (mAbs): FITC anti-CD16 (CLB/FcGran1), PE anti-CD56 (MY31), PerCP-Cy5.5 anti-CD3 (SK7), and V450 anti-CD45 (2D1), all from BD Biosciences. The absolute number of lymphocytes was obtained from the hemogram. The absolute number of NK cells per microliter of blood was calculated using the following formula: (percentage of NK cells within the lymphocyte gate × absolute number of lymphocytes)/100.

DNA extraction, HLA, and KIR genotyping

Following the manufacturer´s recommendations, DNA was obtained from PBMCs using the FlexiGen DNA kit (Qiagen). The first step is the addition of lysis buffer to each sample following the Qiagen FlexiGene DNA procedure flowchart. Briefly, cell nuclei and mitochondria were pelleted by centrifugation and resuspended in denaturation buffer containing QIAGEN Protease. Following protein digestion, DNA was precipitated by the addition of isopropanol, recovered by centrifugation, washed in 70% ethanol, and dried. DNA was resuspended in hydration buffer and stored at −20 °C for further use.

HLA-A, B, and C *loci* typing (necessary to discriminate the KIR ligands present in each patient) was performed using the following kits: LIFECODES HLA-A, B SSO Typing Kit and LIFECODES HLA-C eRES SSO Typing Kit (Lifecodes), all of them CE marked. Lifecodes HLA uses PCR-SSO methodology, subsequent data input on the Luminex® 200™ (Merck) analyzer, and results were examined using Matchit DNA software. HLA genotyping was performed at a level of resolution that allowed determining the KIR-binding epitope to distinguish Bw4 specificities and the HLA-C dimorphism at position 80 of the α1 helix. In situations of ambiguity when assigning alleles or to rule out more frequent null alleles, NGS typing was also performed. The NGSgo-MX6 multiplex amplification strategy was used, followed by sequencing on the Illumina Myseq platform and analysis by the NGS engine program.

KIR typing was performed by a PCR-SSP method (sequence-specific primers) using the KIR Ready gene kit (Inno-train Diagnostik GmbH). PCR products were amplified and subsequently resolved on agarose gels, and results were interpreted according to the manufacturer's instructions. Based on KIR gene content, haplotype (A or B) was defined, and genotypes (AA or Bx, where x can be A or B) were grouped for each patient. The AA genotype is homozygous for inhibitory haplotype A (consisting of 3DL3, 2DL3, 2DP1, 2DL1, 3DP1, 2DL4, 3DL1, 2DS4, and 3DL2). Haplotype B or Bx genotype includes any combination of KIR other than the above.

Determination of cytokines in plasma

Plasma samples were obtained from blood samples and stored at −80 °C until they were required. For the measurement of IL-15, PDGF-DD, and PDGF-BB plasma levels, the human IL-15, PDGF-DD, or PDGF-BB Quantikine ELISA Kits (R&D Systems) were used, respectively, following the manufacturer's recommendations. The optical density was determined using a Varioskan Flash fluorimeter (Thermo Fisher Scientific), and the standard curve and non-linear regression, and log-log line model were performed in GraphPad Prism software. For the measurement of TGF-β plasma levels, Luminex MILLIPLEX TGF-beta 1 Single Plex MAGNETIC Bead Kit (Merck) was used, following the manufacturer's recommendations. Levels of TGF-β were quantified using Luminex® 200™ (Merck) and analyzed using xPONENT® software. For the determination of GDF-15 and placental growth factor (PlGF) plasma levels, Elecsys GDF-15 and Elecsys PlGF kits (Roche) were used, following the manufacturer's recommendations. For quantification, the electrochemiluminescence was determined in a Cobas e 801 analytical unit (Roche) immunoassay analyzer.

NK cell culture with cytokines

For in vitro experiments, 1.5×10^6 PBMCs/mL were cultured in a 48-well plate in 1 mL of NK cell culture media (described above) with different combinations of IL-15 (10 ng/mL) and TGF-β (1–10 ng/mL) cytokines. We performed the following conditions: no cytokines (unstimulated), IL-15, 5 ng/mL TGF-β, IL-15 + 1 ng/mL TGF-β, IL-15 + 5 ng/mL TGF-β and IL-15 + 10 ng/mL TGF-β. Cells were cultured for 7 days, and the media was refreshed at day 4. For the scRNA-seq experiment, PBMCs were cultured in NK cell media without cytokines or with a combination of IL-15 (10 ng/mL) and TGF-β (5 ng/mL) for 4 days.

scRNA-seq

Four single-cell RNA libraries were constructed using a Chromium controller (10x Genomics, Pleasanton, CA, USA) as per the manufacturer's instructions (10x Genomics Chromium Single Cell 3′ V3.1 chemistry). A total of 12 cDNA amplification cycles and 14 cycles of library amplification were performed. Sequencing was carried out using a Novaseq 6000 SP Reagent Kit v1.5 (Illumina, San Diego, CA, USA; 100 cycles). FASTQ sequence data were aligned to a custom hg38 (GRCh37, CellRanger reference genome version References- 2020-A, build GRCh38.p13) using CellRanger count (v7.2.0).

Gene counts were loaded into R (R-project.org/, v4.3.1) using Seurat (v5.0.1). Analysis was conducted with Seurat and extensive use of dplyr (v1.1.4) and tidyverse (v2.0.0) functionality. For each of the four libraries analyzed, we filtered poor-quality cells by requiring each cell to have at least 800 expressed genes (of at least one count), at most 40,000 reads (removing cell doublets), and at most 10% mitochondrial RNA (removing dying cells). We then proceed with the normalization, variable feature identification, scaling of the data, and principal component analysis (PCA) of each of the libraries. We next integrated the libraries with the CCA integration method using the IntegrateLayers function in Seurat. Uniform manifold approximation and projection (UMAP) dimensionality reductions were produced, and clusters were computed with the FindNeighbours function, followed by FindClusters (resolution of 0.6), resulting in 18 clusters. In addition, the phateR (v1.0.7) package was used to calculate 2-dimensional PHATE embeddings from the normalized data.

For the NK cell population, we further annotated cell type clusters of NK cells (clusters 7 and 9) by sub-setting the Seurat object to these cells only, and then repeating the procedure described above, but with only 20 dimensions for the UMAP and clustering. With this, NK cells were further

divided into 9 clusters representing NK1, NK2, NK3, and NK4 cells, using expression patterns and marker gene lists. For each NK cell (sub)type, we compared gene expression levels between cells untreated and treated with IL-15 + TGF-β, using the FindMarkers function in Seurat on the normalized counts (Seurat RNA Assay). UMAP and PHATE cell embeddings were visualized using the function Dimplot in Seurat. Gene expression was visualized using Featureplots and dotplots in Seurat.

Flow cytometry

For flow cytometry analysis of NK cells, PBMCs were first stained with LIVE/DEAD Fixable Aqua Dead Cell Stain Kit (Invitrogen) reagent to exclude dead cells, following the manufacturer´s recommendations. Then, cells were washed with PBS containing 2.5% bovine serum albumin (BSA, Sigma-Aldrich) before performing surface receptor staining. For that, cells were incubated for 30 min on ice, in the dark, with the fluorochrome-conjugated mAbs summarized in Tables S1–S4 (for phenotypical analysis, three different panels were used, numbered from 1 to 3 in Tables S1–S3, and an additional panel for in vitro experiments in Table S4). After staining, cells were then washed again with PBS containing 2.5% BSA and resuspended in PBS. Samples were acquired in a LSR Fortessa X-20 flow cytometer (BD Bioscience).

Flow cytometry data analysis

Flow cytometry data were analyzed using FlowJo v10.8.1. software. Manual and automated analyses were performed. The following plug-ins were used: DownSample (1.1), UMAP, t-SNE, and FlowSOM (2.6). Briefly, for the automated analysis, events were first downsampled from the gate of interest (NK cells) across all samples using the DownSample plug-in and concatenated. For each donor, NK cells were downsampled to 157 cells in the case of the FlowSOM of Fig. 2 and 1510 cells in the FlowSOM of Fig. 6. Then, downsampled populations were concatenated for the analysis. FlowSOM was run using the indicated parameters in each figure.

Statistics and reproducibility

Statistical analyses were performed as described in the figure legends. GraphPad Prism v.9.3.1 was used for graphical representation and statistical analysis. Non-parametric Wilcoxon matched-pairs signed-rank test was used to determine significant differences among groups, and Mann–Whitney unpaired test was used to determine significant differences among non-paired data. The Rout test was used in the case of the HLA-DR marker in order to identify outliers in the $CD56^{neg}$ population.

Correlation plots between different variables were calculated and visualized as correlograms. The Pearson correlation coefficient was indicated by square size and heat scale. These analyses were performed with R (version 4.3.1): A language and environment for statistical computing (R Foundation for Statistical Computing, Vienna, Austria).

Reporting summary

Further information on research design is available in the Nature Portfolio Reporting Summary linked to this article.

Results

NK cell counts, subset frequencies, and maturation status after autoHSCT

NK cell phenotype changes during the immune system reconstitution after autoHSCT[8,15,16,19]. In this work we have studied the NK cell reconstitution in a cohort of 13 pediatric patients with cancer undergoing autoHSCT using blood samples taken at different time points: before autoHSCT (S1), after reaching leukocyte recovery (>1000 leukocytes/μl, usually around day 12 after autoHSCT, S2) and 30 days (S3), 100 days (S4), and 180 days (S5) after autoHSCT. Patients' clinical characteristics are described in Table 1. After autoHSCT, absolute number of NK cells did not significantly change, although a reduction was noticed from S1 to S2, followed by a sustained increase until S5 (Fig. 1a). The percentage of NK cells within lymphocytes did not change during the reconstitution. To characterize NK cells, we defined them by the expression of NKp80 and CD56, and the negative expression of other cell markers (CD3, CD14, CD19, and CD123), as it is shown in Fig. S1. We also defined 3 different NK cell subsets based on the expression of the CD56 marker: $CD56^{bright}$, $CD56^{dim}$, and $CD56^{neg}$[27], and we observed that after autoHSCT, their percentage did not overly fluctuate (Fig. 1b).

The frequency of NKG2A+ NK cells increased early after transplantation (from S1 to S2) (Fig. 1c). In contrast, the frequency of CD57+ NK cells increased at later time points (>100 days, S4 and S5) (Fig. 1d). Also, the co-expression of NKG2A and CD57 was analyzed after autoHSCT for all NK cell subsets. As expected, the results showed that, not only the most immature $CD56^{bright}$ subset were mostly NKG2A+CD57−, but also that these NKG2A+CD57− cells represent the most frequent subset within the total NK cells in these children (Fig. 1e). Overall, we observed that after autoHSCT there is a gradual decrease in the frequency of immature NK cells (NKG2A+CD57−), while the percentage of terminally differentiated (NKG2A−CD57+) NK cells increased. Nevertheless, the more immature subset (NKG2A+CD57−) is the predominant at every analyzed time point (Fig. 1e, f).

NK cell receptor repertoire is altered following autoHSCT

It was previously reported that genes associated with activation, cytotoxic functions, and several receptors were differentially expressed in adult MM patients after autoHSCT[17]. Hence, we decided to study the expression of these and other molecules in NK cell subsets in our pediatric cohort. The activating co-receptor and activation marker CD38[28] is practically expressed by all NK cell subsets, and its expression increased early after autoHSCT (S2), while from day 30 (S3) onwards, the expression gradually decreased to the initial levels (Fig. 2a). Similarly, autoHSCT induces a transient increase of NK cells expressing HLA-DR and CD26 (Fig. 2a), which have been described as functionally more activated cells[29,30]. On the other hand, regarding the cytotoxicity-associated marker CD8[31], the transient increase at S2 was only observed in the $CD56^{bright}$ NK cell subset (Fig. 2a).

In addition, results also showed that NK cells expressed higher levels of CD31 and LAIR-1 inhibitory receptors at S2 compared to other time points (Fig. 2b). CD55, a marker expressed at higher levels on $CD56^{bright}$ NK cells[32], followed the same trend (Fig. 2b). However, regarding activating receptors, the percentage of CD160+ NK cells decreased at S2, as well as the expression of CD229 and 2B4 (also known as CD244) (Fig. 2c). Lastly, the expression of other receptors, such as Siglec-7, TIM3 and CD226 (DNAM-1) did not significantly change after transplantation (Fig. S2a).

We performed an unsupervised analysis using UMAP and FlowSOM clustering methodology (Fig. 2d). Among CD56+ NK cells, the analysis revealed 8 populations (or Pops) based on the expression of 10 cell surface markers (CD8, CD26, CD31, CD38, CD55, CD160, CD226, CD229, HLA-DR and LAIR-1). We observed a significant increase in the frequency of Pop 7 at S2 corresponding to NK cells expressing high levels of CD26, CD55, HLA-DR, CD38, CD31, and LAIR-1, and low levels of CD229 and CD160. We also observed a significant decrease of Pop 1 at S2 corresponding to NK cells which express high levels of CD229 and CD160, and low levels of CD26, CD55, HLA-DR, CD31, and LAIR-1. Altogether, these results indicate that, early after autoHSCT, NK cells are more activated and that their receptor repertoire is biased towards an inhibitory phenotype, as it was reflected by the transient increase in the expression of inhibitory receptors and the decrease of activating receptors.

To determine whether the previous data are clinically relevant, we performed correlation analyses between the expression of different markers and relapse in the cohort of pediatric patients undergoing an autoHSCT (Fig. S2b). We observed a negative correlation between relapse and percentage of $CD56^{bright}$ NK cells early after autoHSCT (S2) and, as expected, a positive correlation between relapse and percentage of $CD56^{dim}$ NK cells. This could indicate that patients with a higher

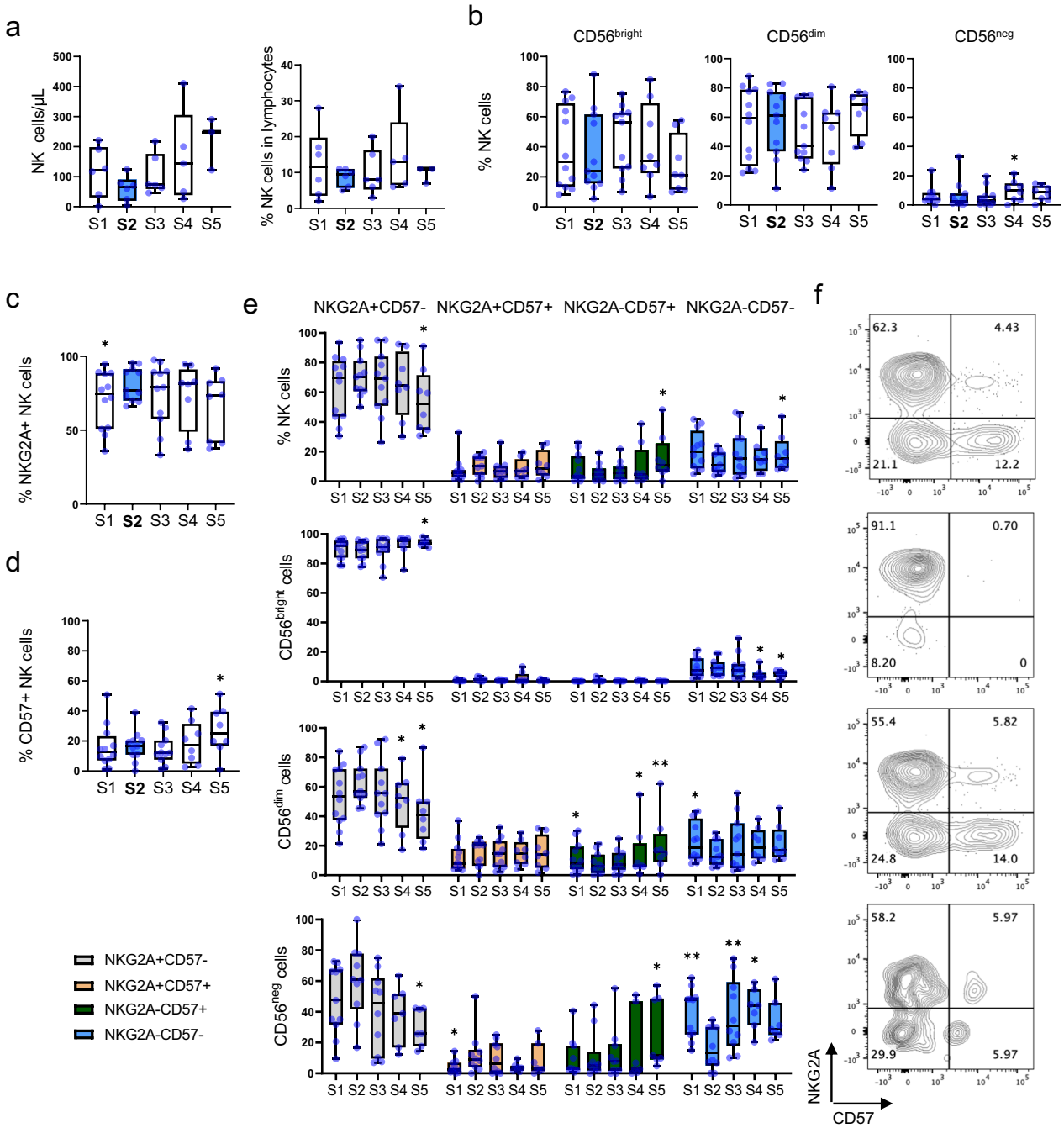

Fig. 1 | NK cell numbers, subsets, and maturation status after autoHSCT. Boxplot graphs showing the analysis of NK cells at the studied five time points: before autoHSCT (S1), after reaching leukocyte recovery (more than 1000 leukocytes/μl, usually around day 12 after autoHSCT) (S2), 30 days (S3), 100 days (S4), and 180 days (S5). **a** Absolute number of NK cells (left) and percentage of NK cells within lymphocytes (right). Each dot represents a patient (S1 $n = 6$; S2 $n = 6$; S3 $n = 6$; S4 $n = 5$; S5 $n = 3$). **b** Percentage of NK cell subsets based on CD56 expression, including $CD56^{bright}$, $CD56^{dim}$ and $CD56^{neg}$ NK cells. **c**–**e** Analysis of NKG2A and CD57 receptors expression. **c** Percentage of NKG2A-expressing NK cells. **d** Percentage of CD57-expressing NK cells. **e** Percentage of NKG2A+CD57− (gray), NKG2A+CD57+ (yellow), NKG2A−CD57+ (green), NKG2A−CD57− (blue) cells within total NK cells, and $CD56^{bright}$, $CD56^{dim}$, and $CD56^{neg}$ NK cell subsets (left) and **f** representative contour plots showing the four analyzed populations (right). Boxplots show the median and 25–75th percentiles, and the whiskers denote the lowest and highest values. Each dot represents a patient (S1 $n = 12$; S2 $n = 11$; S3 $n = 11$; S4 $n = 8$; S5 $n = 8$ unless otherwise specified). The significance of the data was determined by comparing each sample with sample S2. $^*p < 0.05$, $^{**}p < 0.01$ (Wilcoxon matched-pairs signed-rank test). Exact p values are provided in a file named Supplementary Data 2, under Fig. 1.

frequency of mature ($CD56^{dim}$) NK cells at S2 could have a worse outcome after autoHSCT. On the other hand, CD26 and CD55 expression levels at S2 were negatively associated with relapse. The relevance of these data is difficult to determine given the number and heterogeneity of the patients. Clearly, larger and more homogeneous cohorts of patients are needed to validate these results.

KIR expression was temporarily increased shortly after autoHSCT

KIRs regulate NK cell ability to recognize and kill tumor cells; their expression is associated with the outcome of patients with different types of cancer, including neuroblastoma[26], and following HSCT, there are changes in their expression[15,17]. Therefore, we decided to study KIR

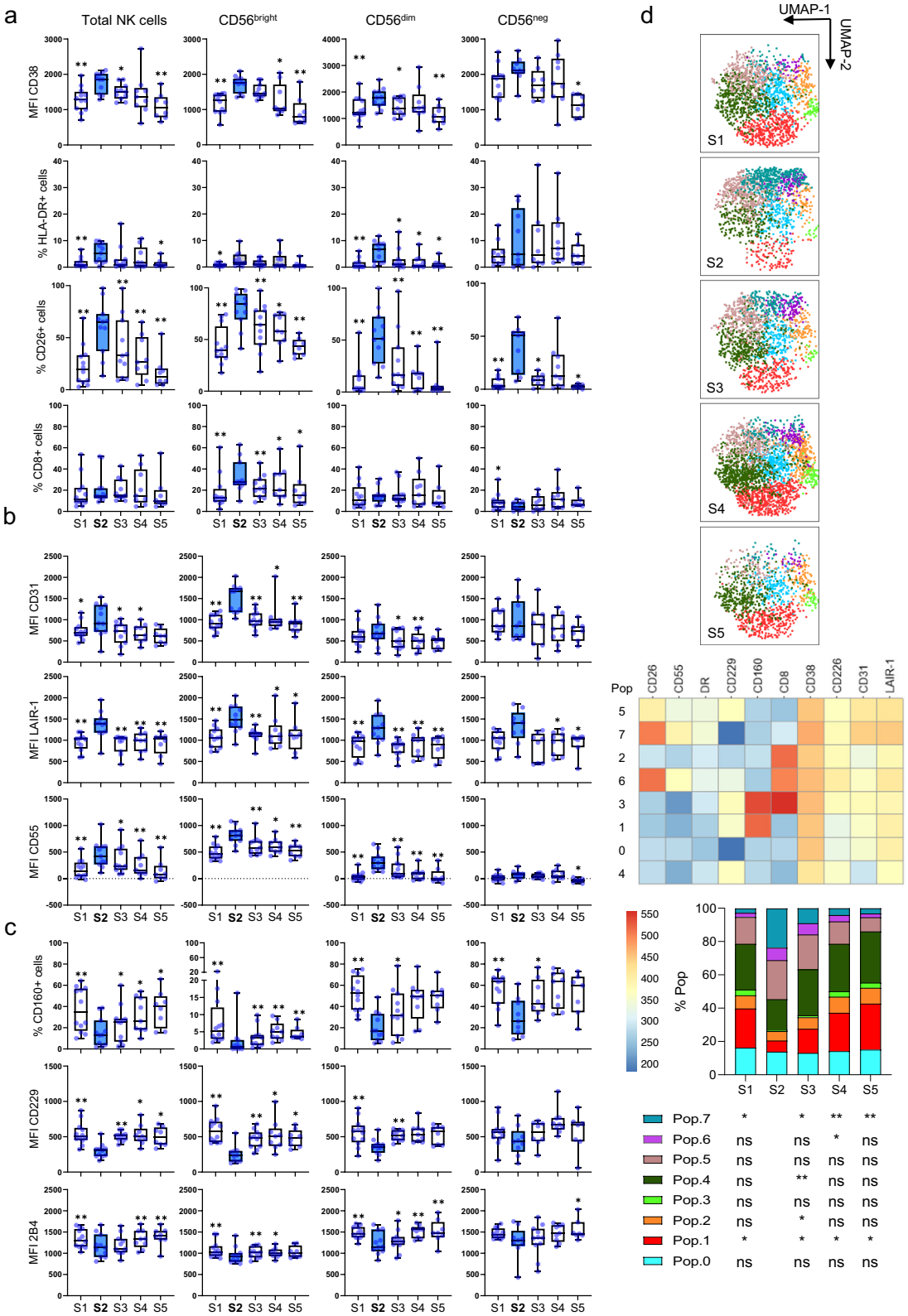

expression in our cohort. Firstly, we analyzed the patients´ KIR haplotype (Table S5). Next, we analyzed KIR expression only in the patients who have the genes encoding the corresponding KIRs. We observed an increase in the percentage of KIR3DL1+ cells early after autoHSCT in total NK cells, and an increase of KIR2DL1 and KIR2DL2/L3/S2, only in the CD56^{bright} NK cell subset (Fig. 3a). However, we did not see significant variations regarding KIR2DS4 after transplant (Fig. S3), a gene expressed only in three patients (Table S5).

During NK cell differentiation, CD56^{dim} NK cells gradually decrease NKG2A and increase CD57 and KIR expression[33]. Thus, we next analyzed within different NK cell subsets, the number of KIR (KIR3DL1, KIR2DL2/L3/S2, and KIR2DL1) that NK cells expressed. First, we observed a

Fig. 2 | NK cell receptor repertoire following autoHSCT. Analysis of NK cells in a cohort of pediatric patients before (S1) and following autoHSCT: after reaching leukocyte recovery (more than 1000 leukocytes/µl, usually around day 12 after autoHSCT) (S2), 30 days (S3), 100 days (S4), and 180 days (S5). **a** Boxplot graphs showing the median fluorescence intensity (MFI) of CD38 expression and the percentage of cells expressing HLA-DR, CD26, and CD8 within total NK cells and NK cell subsets based on CD56 expression, including CD56^{dim}, CD56^{bright}, and CD56^{neg} NK cells. **b** MFI of CD31, LAIR-1 and CD55 expression. **c** Percentage of CD160+ cells and MFI of CD229 and 2B4 expression. Boxplots show the median and 25–75th percentiles, and the whiskers denote the lowest and highest values. Each dot represents a patient. A minimum of 10 cells were analyzed in each cell subset. S1 $n = 12$; S2 $n = 11$; S3 $n = 11$; S4 $n = 9$; S5 n = 8 for total, CD56^{bright} and CD56^{dim} NK cells. S1 $n = 11$; S2 $n = 9$; S3 $n = 8$; S4 $n = 9$; S5 $n = 7$ for CD56^{neg} NK cells, except for the 2B4 marker (S1 $n = 12$; S2 $n = 9$; S3 $n = 11$; S4 $n = 9$; S5 $n = 7$). **d** UMAP projection of CD56+ NK cell populations (Pop) identified by the FlowSOM clustering tool for the specified markers, fluorescence intensity of each Pop as indicated in the column-scaled *z*-score, and bars graph showing the percentage of each Pop at the studied five time points (S1–S5). Results were compared with the S2 time point using the Wilcoxon matched-pairs signed-rank test. $^{*}p < 0.05$, $^{**}p < 0.01$ and ns no significant. Exact *p* values are provided in a file named Supplementary Data 2, under Fig. 2.

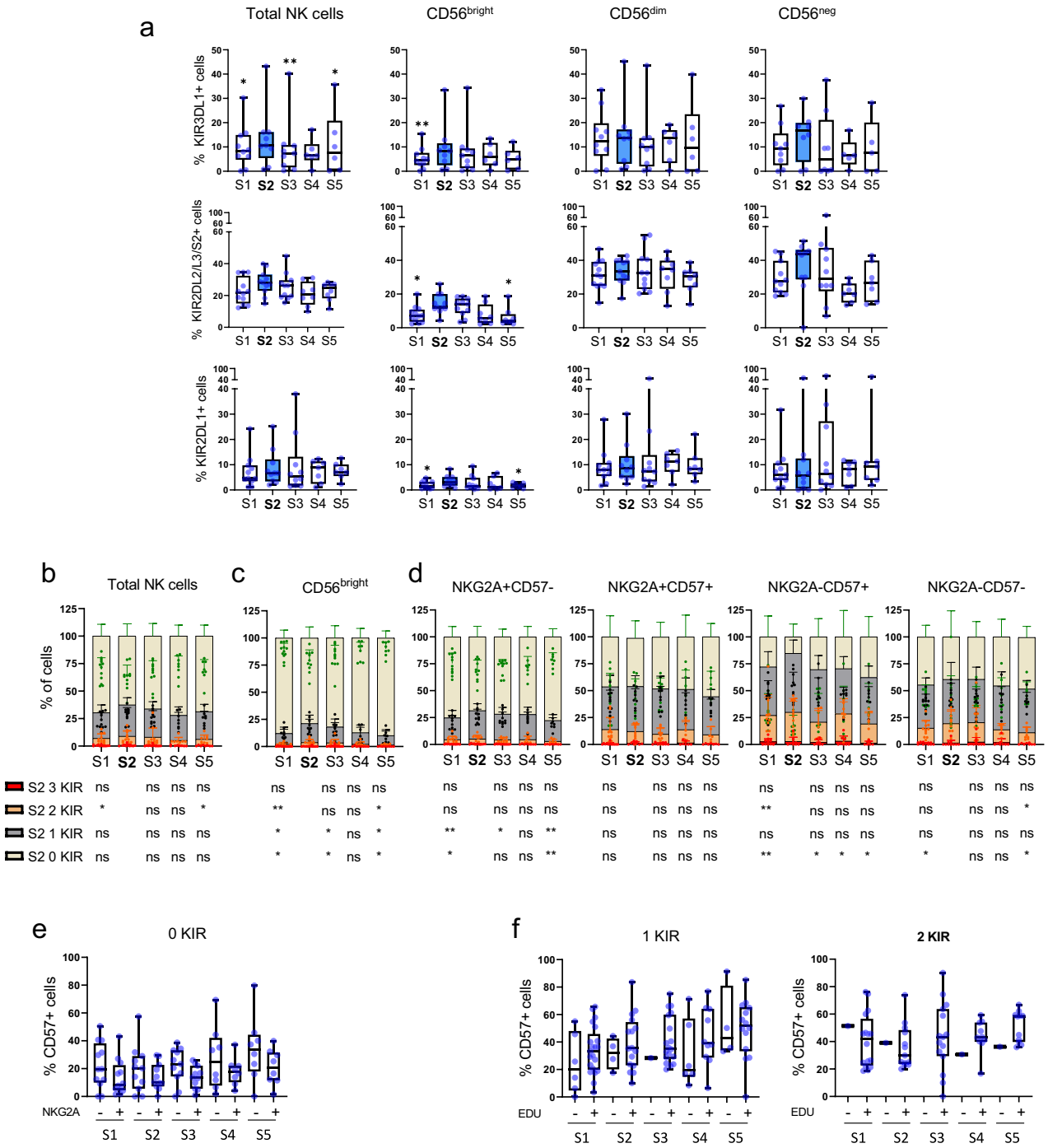

Fig. 3 | NK cell KIR expression is altered after autoHSCT, and NK cell education is not coupled with terminal differentiation a Boxplot graphs showing, at the studied five time points (S1–S5), the percentage of cells expressing KIR3DL1 (S1 $n = 10$; S2 $n = 9$; S3 $n = 9$; S4 $n = 6$; S5 $n = 6$), KIR2DL2/L3/S2 (S1 $n = 12$; S2 $n = 11$; S3 $n = 11$; S4 $n = 8$; S5 $n = 8$) and KIR2DL1 (S1 $n = 11$; S2 $n = 10$; S3 $n = 10$; S4 $n = 7$; S5 $n = 7$) within total NK cells and NK cell subsets based on CD56 expression, including $CD56^{dim}$, $CD56^{bright}$ and $CD56^{neg}$ NK cells. Boxplots show the median and 25–75th percentiles, and the whiskers denote the lowest and highest values. The significance of the data was determined by comparing each sample with sample S2. Each dot represents a patient. $^{*}p < 0.05$, $^{**}p < 0.01$. No significance was not indicated (Wilcoxon matched-pairs signed-rank test). **b–d** Bar graphs showing the percentage of cells expressing 0 (green), 1 (gray), 2 (orange), or 3 (red) KIR (KIR2DL1, KIR2DL2/L3/S2, and KIR3DL1) at the studied five time points (S1–S5). Analysis of KIR combinations in total NK cells (**b**), $CD56^{bright}$ NK cells (**c**), and $CD56^{dim}$ NK cell subsets based on the expression of NKG2A and CD57 (**d**). Data are represented as the mean + SD. (S1 $n = 12$; S2 $n = 11$; S3 $n = 11$; S4 $n = 8$; S5 $n = 8$). Results were compared with the S2 time point using the Wilcoxon matched-pairs signed-rank test. Each dot represents a patient. $^{*}p < 0.05$, $^{**}p < 0.01$ and ns no significant. **e**, **f** Boxplot graphs showing the percentage of CD57+ cells at the studied time points on KIR- (0 KIR), 1 KIR or 2 KIR $CD56^{dim}$ NK cell subsets. Percentage of CD57+ cells in KIR-NKG2A+ or KIR-NKG2A- $CD56^{dim}$ NK cells at different time points (**e**). Percentage of CD57+ cells in educated (EDU+) or uneducated (EDU−) $CD56^{dim}$ NK cells with 1 or 2 KIR (**f**). Single KIR-positive cells were considered educated if the KIR is specific for the HLA class I haplotype in a given patient (Tables S5 and S6). Double KIR-positive cells were considered educated if they had at least one KIR that is specific for the HLA class I haplotype in that particular patient (Tables S5 and S6). Data are represented as the median and 25–75th percentiles, and the whiskers denote the lowest and highest values (S1 $n = 12$; S2 $n = 11$; S3 $n = 11$; S4 $n = 8$; S5 $n = 8$ were analyzed, but only data that followed the education criteria specified above were considered, and more than one value could be added for each patient because NK cells could be educated for more than one KIR). Results were compared between − and + samples for each time point using an unpaired Mann–Whitney test. No significance was not indicated. Each dot represents a patient. Exact p values are provided in a file named Supplementary Data 2, under Fig. 3.

significant increase in NK cells expressing one or two KIR early after transplant (S2), followed by a gradual decrease reaching pre-transplant levels at day 180 (S5) (Fig. 3b). Regarding $CD56^{bright}$ NK cells, there was a significant decrease in KIR negative cells and an increase in one and two KIR expressing cells at S2 (Fig. 3c). Since we have previously seen that the maturation status is altered after autoHSCT (Fig. 1e), especially in $CD56^{dim}$ NK cells, we analyzed the frequencies of cells expressing different KIR combinations among different maturation stages. Immature $CD56^{dim}$ NK cells (NKG2A+CD57−) expressed lower KIR levels compared to mature (NKG2A−CD57+) NK cells (Fig. 3d). In addition, regardless of the maturation status, $CD56^{dim}$ NK cells had significantly fewer non-expressing KIR cells at S2 (Fig. 3d). In conclusion, there is a higher KIR expression in mature terminally differentiated $CD56^{dim}$NKG2A-CD57+ NK cells and higher KIR expression early after autoHSCT at S2 in all NK cell subsets.

Finally, as we previously observed a reduction in the frequency of immature (NKG2A+CD57−) NK cells and an increment of mature (NKG2A−CD57+) NK cells later after transplant at S5 (Fig. 1e), we determined whether the process of education by KIRs and NKG2A can influence the expression of CD57, a marker of terminal differentiation, in our pediatric cohort, as it has been studied in alloHSCT[33]. The education status of these subsets was determined by analyzing KIR and HLA genotypes in every patient (Table S6). In this context, NK cells were considered as educated if their KIRs were specific for self-HLA-I molecules. In each patient, we determined the number of educated and uneducated $CD56^{dim}$ NK cells expressing 1 or 2 KIR, and we analyzed the expression of the CD57 receptor. In NK cells lacking KIRs, the expression of CD57 was compared between NKG2A+ and NKG2A− cells (Fig. 3e). Single KIR-positive NK cells were considered educated if the patient expressed the HLA-I ligand for this KIR, and double KIR-positive NK cells were considered educated if the patient expressed at least one HLA-I ligand. The results showed no significant differences in CD57 expression between educated and uneducated subsets after autoHSCT for any number of KIRs studied (Fig. 3f). We conclude that NK cell education and maturation are uncoupled processes during immune reconstitution following autoHSCT.

Transient acquisition of a decidual-like phenotype by NK cells early after autoHSCT

Next, we analyzed the expression of decidual NK cell markers in the pediatric cohort during immune reconstitution, since we have previously discovered that genes codifying CD9 and CD151, two receptors associated with decidual NK cells[34,35], were overexpressed in adult MM patients after autoHSCT[17]. We observed a temporary increase in both CD9 and CD151 expressing NK cells at S2, decreasing to pre-transplant levels at S5 (Fig. 4a). This sharp increase is clearly evidenced at S2 where the double positive (CD9+CD151+) NK cell subset is 4 times higher than at S1, which is contrasting to the small increase observed for CD9+CD151− NK cells (Fig. 4b). This result is consistent among all NK cell subsets ($CD56^{bright}$, $CD56^{dim}$ and to a less extent in $CD56^{neg}$). In our cohort, we observed that CD151+ cells expressed lower levels of CD56 than CD151- cells (Fig. 4c). Additionally, we analyzed CD49a, another decidual NK cell marker[34,36], and we observed low expression levels that, nevertheless, were significantly increased early after autoHSCT (Fig. 4d). Altogether, these results suggest that, following autoHSCT, NK cells acquire a decidual-like phenotype supporting previous results at the transcriptomic level[17].

Plasma cytokine profile following autoHSCT

We have hypothesized that the cytokine *milieu* that is present immediately after autoHSCT may be responsible for the acquisition of a decidual-like phenotype by NK cells. Therefore, to address this question, we have measured the plasma levels of molecules with important roles in NK cell biology and that may have an impact in the expansion of a decidual-like NK cell subset during autoHSCT. IL-15 is a cytokine with a relevant role in proliferation, development, cytotoxic activity, and cytokine production of NK cells[37–39]. Similar to what we and others previously described in adult patients[16,40], we found that IL-15 plasma levels also significantly increased early after autoHSCT in our pediatric cohort (Fig. 5a). Interestingly, we found a positive correlation between IL-15 levels at S2 and the expression of HLA-DR, CD26, CD55 and CD38 (Fig. 5b). These markers also increased at S2, suggesting that increased levels of this cytokine are, at least partially, responsible for the activation phenotype of NK cells at S2.

TGF-β has been shown to modulate NK cells' receptor repertoire and to inhibit NK cell-mediated cytotoxicity, favoring immune evasion[41–45]. In our cohort, we observed that plasma levels of TGF-β slightly decreased, although it was not statistically significant (Fig. 5a). Additionally, a negative correlation was observed at S2 between plasma levels of TGF-β and the increased expression of CD26 and CD31 (Fig. 5b). On the other hand, we also analyzed the plasma levels of growth differentiation factor 15 (GDF-15), which has a role in the development of NK cell dysfunction during systemic inflammation[46]. We found that GDF-15 levels significantly increased at S2 (Fig. 5a) and that positively correlated with the frequency of CD9+ NK cells (Fig. 5b), a subset that is very elevated at S2.

PlGF is a pleiotropic cytokine which regulates the maturation of uterine NK cells and upregulates the expression of other angiogenic factors[47]. PlGF levels significantly increased at S2 (Fig. 5a). However, no significant association of PlGF levels with CD9+ NK cells, or any other NK cell subset, was observed (Fig. 5b). Platelet-derived growth factors (PDGFs) are relevant mitogens for many cell types[48] and many tumors use them as an autocrine signal for proliferation[49]. NK cells express receptors for these molecules[50] and PDGF-BB has been described to be associated with PFS in NHL patients who have undergone autoHSCT[40]. In our cohort, the plasma levels of PDGF-BB and PDGF-DD significantly decreased early after autoHSCT (Fig. 5a). Also, we observed a negative correlation at S2 between these

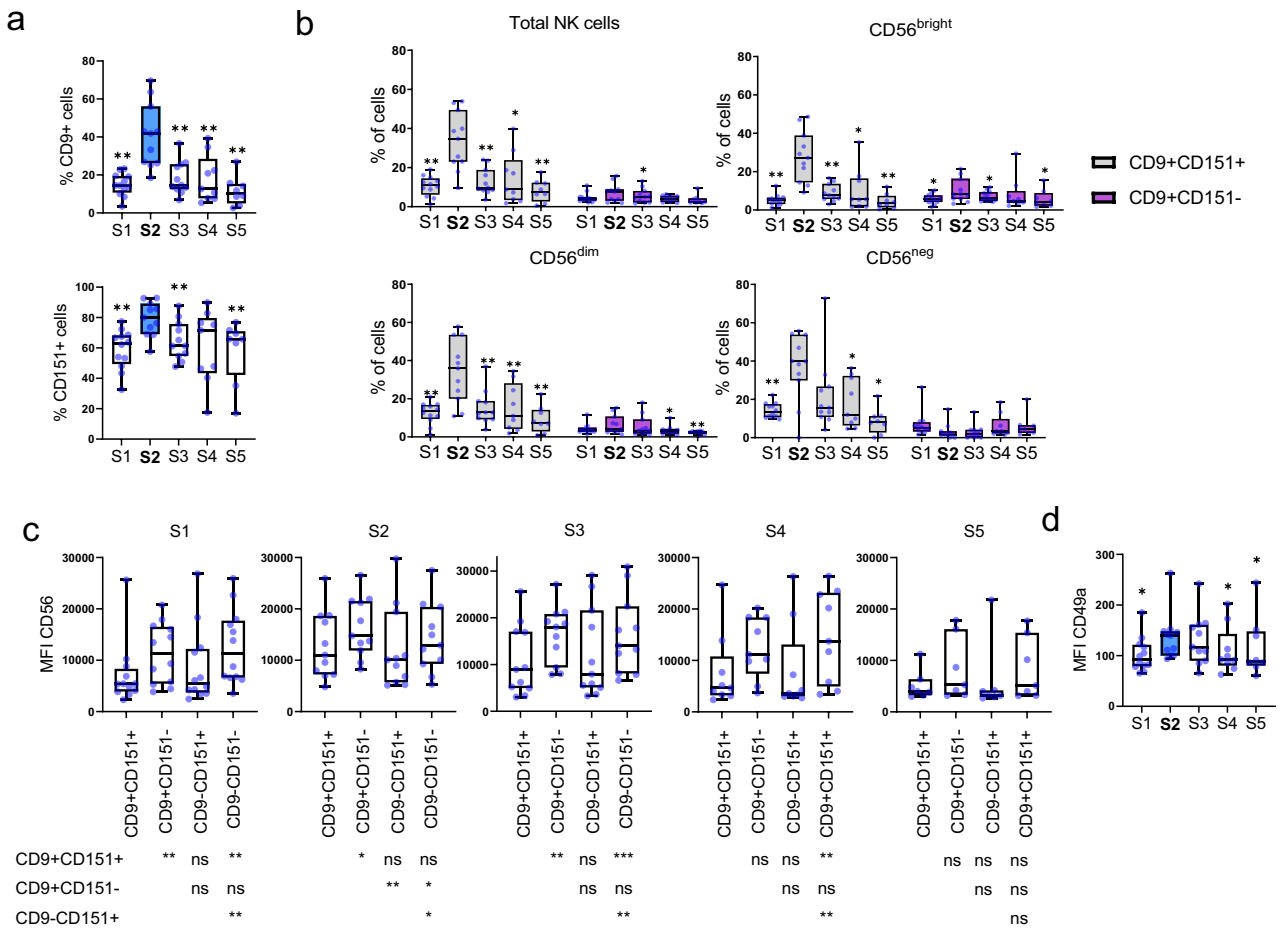

Fig. 4 | Transient acquisition of decidual-like phenotype by NK cells early after autoHSCT. Boxplot graphs showing the analysis of total NK cells and NK cell subsets based on CD56 expression, including CD56^{dim}, CD56^{bright}, and CD56^{neg} NK cells at the five studied time points (S1–S5). **a** Percentage of cells expressing CD9 (upper graph) and CD151 (lower graph) in total NK cells. **b** Percentage of CD9+CD151+ (gray) and CD9+CD151− (purple) within total NK cells and in the three NK cell subsets. **c** Median fluorescence intensity (MFI) of CD56 in CD9+CD151+, CD9+CD151−, CD9−CD151+, and CD9−CD151− in CD56+ NK cells. **d** MFI of CD49a in total NK cells. Data are represented as the median and 25–75th percentiles, and the whiskers denote the lowest and highest values. Each dot represents a patient (S1 $n = 12$; S2 $n = 11$; S3 $n = 11$; S4 $n = 9$; S5 $n = 8$). Results were compared with the S2 time point using the Wilcoxon matched-pairs signed-rank test. $^{*}p < 0.05$, $^{**}p < 0.01$ and ns no significant. Exact p values are provided in a file named Supplementary Data 2, under Fig. 4.

PDGFs and the expression levels of CD31, as well as the frequencies of CD26+ and CD9+CD151+ NK cells (Fig. 5b), which were increased at this point. To sum up, early after autoHSCT, IL-15, GDF-15, and PlGF levels increase, PDGF-BB and PDGF-DD levels decrease, while the concentration of TGF-β in plasma does not change.

IL-15 and TGF-β cooperate to induce a decidual-like phenotype on NK cells

Given that others have shown that the combination of TGF-β with IL-15 induced the acquisition of decidual NK cell markers[51,52], we have considered the possibility that a combination of cytokines may be required for the expansion of the decidual-like NK cell subset. Therefore, we performed in vitro experiments to determine whether the combination of these two cytokines recapitulates the NK cell phenotype observed after autoHSCT, including the decidual-like subset expansion, at S2. To study the effect of IL-15 and TGF-β at single-cell resolution, we performed a single-cell RNA sequencing experiment (scRNA-seq) on PBMC cells from a healthy donor cultured with and without IL-15 (10 ng/mL) + TGF-β (5 ng/mL). PCA and UMAP mapped these cells into 18 clusters representing the mayor immune cell populations, including B and T cells, monocytes, NK cells, and others (Fig. 6a). By further sub-clustering NK cells, we identified 4 different NK subpopulations, namely NK1, NK2, NK3, and NK4 (Fig. 6b). We followed the nomenclature described by Crinier et al[53]., and NK1 corresponded to CD56 ^{dim} and NK2 to CD56^{bright} NK cells. NK1 cells were exclusively present on unstimulated NK cells, while NK2 cells were observed in both unstimulated and IL-15 + TGF-β-treated NK cells. On the other hand, the subsets that we have called NK3 and NK4 were almost exclusively observed in IL-15 + TGF-β-treated NK cells.

We used a complementary method of dimensionality reduction, namely PHATE (Potential of Heat-diffusion for Affinity-based Transition Embedding), to further visualize the NK cells, and observed that the NK4 cluster was only distantly related to the cluster NK1, suggesting that cytokine stimulation has triggered a transcriptional program that significantly differs from the one observed in unstimulated NK cells (Fig. 6c). Determination of the cell cycle state based on the expression of G2/M and S phase markers, indicated that while the majority of NK4 cells were in the cycling phases (G2/M and S), only 49% and 64% of cells in the NK3 and NK2 clusters, respectively, were actively cycling. Virtually none were observed in the NK1 cluster (Fig. 6d–f). Finally, we analyzed the expression levels of genes that encoded cell surface markers that significantly changed early after autoHSCT (S2) in our cohort of pediatric patients. We observed significant upregulation of *DPP4* (CD26), *CD9* (CD9), *ITGA1* (CD49a) and *CD8A* (CD8) in treated cells, and downregulation of *CD160* (CD160) and *CD244* (2B4) (Fig. 6g–i), consistent with what has been observed at the protein level

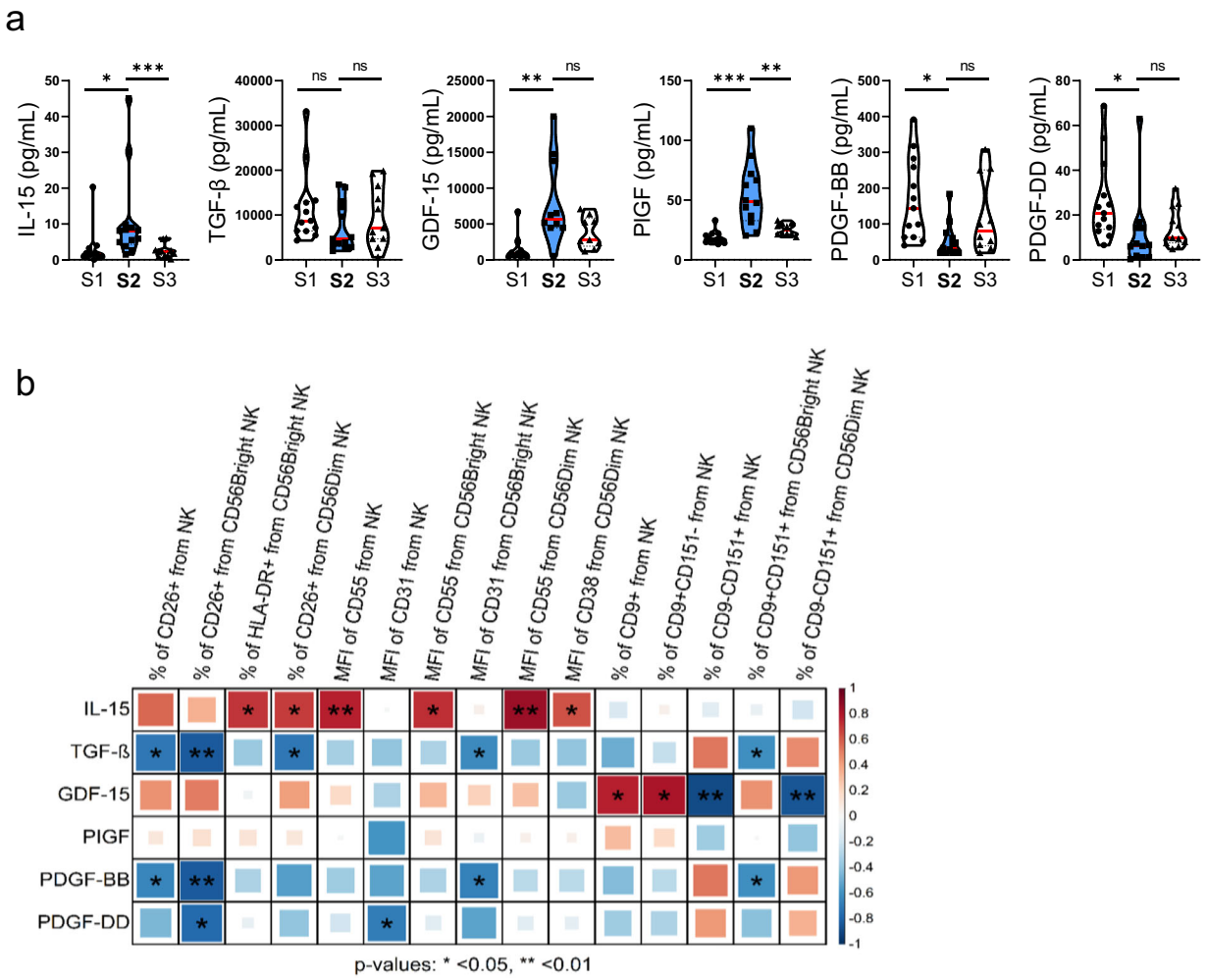

Fig. 5 | Cytokines plasma levels are altered early after autoHSCT. a Violin plots showing IL-15, TGF-β, GDF-15, PlGF, PDGF-BB, and PDGF-DD plasma levels in a cohort of pediatric patients before (S1) and after autoHSCT: after reaching leukocyte recovery (more than 1000 leukocytes/µl, usually around day 12 after autoHSCT) (S2) and 30 days (S3). Data are represented with the median (red). Each dot represents a patient (S1 $n = 13$; S2 $n = 13$; S3 $n = 13$). Results were compared with the S2 time point (blue) using the Wilcoxon matched-pairs signed-rank test. $^{*}p < 0.05$, $^{**}p < 0.01$, $^{***}p < 0.001$ and ns, no significant. **b** Correlogram showing Pearson correlation of the indicated flow cytometry data at S2 and IL-15, TGF-β, GDF-15, PlGF, PDGF-BB, and PDGF-DD plasma levels. Pearson correlation coefficient was indicated by square size (higher size means higher coefficient) and heat scale (positive correlation in red and negative correlation in blue): $^{*}p < 0.05$, $^{**}p < 0.01$. Exact p values are provided in a file named Supplementary Data 2, under Fig. 5.

at S2. The significant gene expression changes observed in *CD38* and *PECAM1* did not correlate with cell surface expression of CD38 and CD31, respectively, at S2. Genes encoding other cell surface receptors did not significantly change.

We also isolated PBMCs from several healthy donors and incubated them with IL-15 and TGF-β at increasing concentrations. We studied the following conditions: unstimulated, 5 ng/mL of TGF-β, 10 ng/mL of IL-15 without or with increasing concentrations of TGF-β (1, 5, or 10 ng/mL). NK cells were identified by flow cytometry as viable CD3-/CD14-/CD19-/CD123-/CD56+ cells and were analyzed to determine the differentially expressed receptors. Conventional supervised analyses were performed, and higher CD38, HLA-DR, CD55, CD56, and CD151 expression levels were observed when cells were incubated with IL-15 compared with the unstimulated condition (Fig. S4a–d). On the other hand, TGF-β alone induced a significant decrease in the expression of these markers when compared with unstimulated cells, except for CD151 (Fig. S4a–d). Nevertheless, TGF-β tended to down-regulate IL-15-induced expression of CD38, HLA-DR, CD55, and CD56, but not to the levels of unstimulated NK cells, suggesting that, at these concentrations, IL-15 has a more dominant effect than TGF-β. On the other hand, we observed a higher expression of decidual markers CD9 and CD49a in conditions containing both TGF-β and IL-15, suggesting that both cytokines are necessary in order to obtain high levels of these two markers (Fig. S4d). Moreover, we observed a significantly lower expression of CD160 and CD229 in response to TGF-β and IL-15 (Fig. S4e). The CD160 decrease was even higher when both cytokines were present, suggesting a synergistic effect, while this synergy was not observed when we looked at CD229 expression levels.

To gain more insight, we performed an unsupervised analysis using t-distributed stochastic neighbor embedding (t-SNE) and the FlowSOM clustering tool for total NK cells (Fig. 7). We observed an increase in Pops 0, 3, and 4 when cells were cultured with IL-15 and TGF-β in comparison with the unstimulated condition and single cytokine treatment. These Pops define CD9+CD38+CD56^{high} NK cells that, specifically in Pops 0 and 4, also expressed CD55 and CD151. Pop 4, in particular, exhibited the highest expression of CD49a. Pop 1, with a CD9+CD151−CD56^{low} phenotype, was almost exclusively present when NK cells were cultured only with TGF-β, and Pop 2, with a CD9-CD151-CD56^{low} phenotype, is the most abundant in unstimulated or only TGF-β conditions. These results suggest that TGF-β is necessary for the expression of CD9 and that IL-15 is responsible for the increased expression of CD56, CD151, CD49a, CD38, and CD55. Within

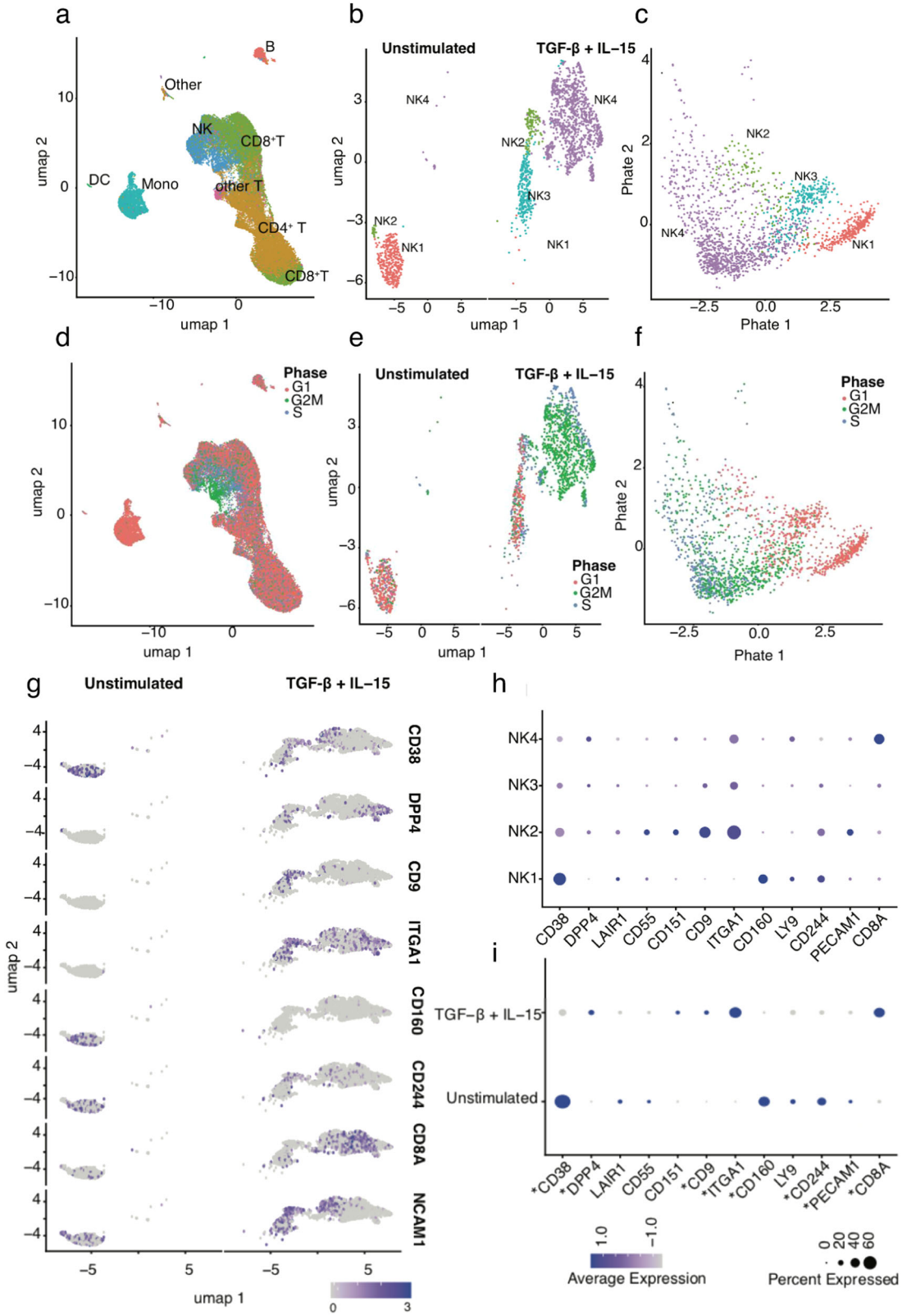

Fig. 6 | Transcriptome of NK cells in vitro cultured with IL-15 and TGF-β. scRNA-seq-based clustering and cell type identification of 30,842 cells from unstimulated versus stimulated PBMCs shown by a UMAP embedding, colored by the predicted cell type (**a**) and cell cycle phase (**d**). Clustering and cell subtype identification of a subset of 1708 NK cells (unstimulated and stimulated) as shown by the UMAP (**b**, **e**) and PHATE embeddings (**c**, **f**), color coded by cell subtype (**b**, **c**) and cell cycle phase (**e**, **f**). UMAP embedding showing expression levels of relevant genes showing differentially significant expression in treated vs unstimulated cells. The panels show unstimulated (left) and stimulated (right) NK cells (**g**). Dot plot of relevant genes. The size of the dots is proportional to the percentage of cells that express a given gene within a cell type, while the color of the dot corresponds to the scaled average gene expression (**h**, **i**).

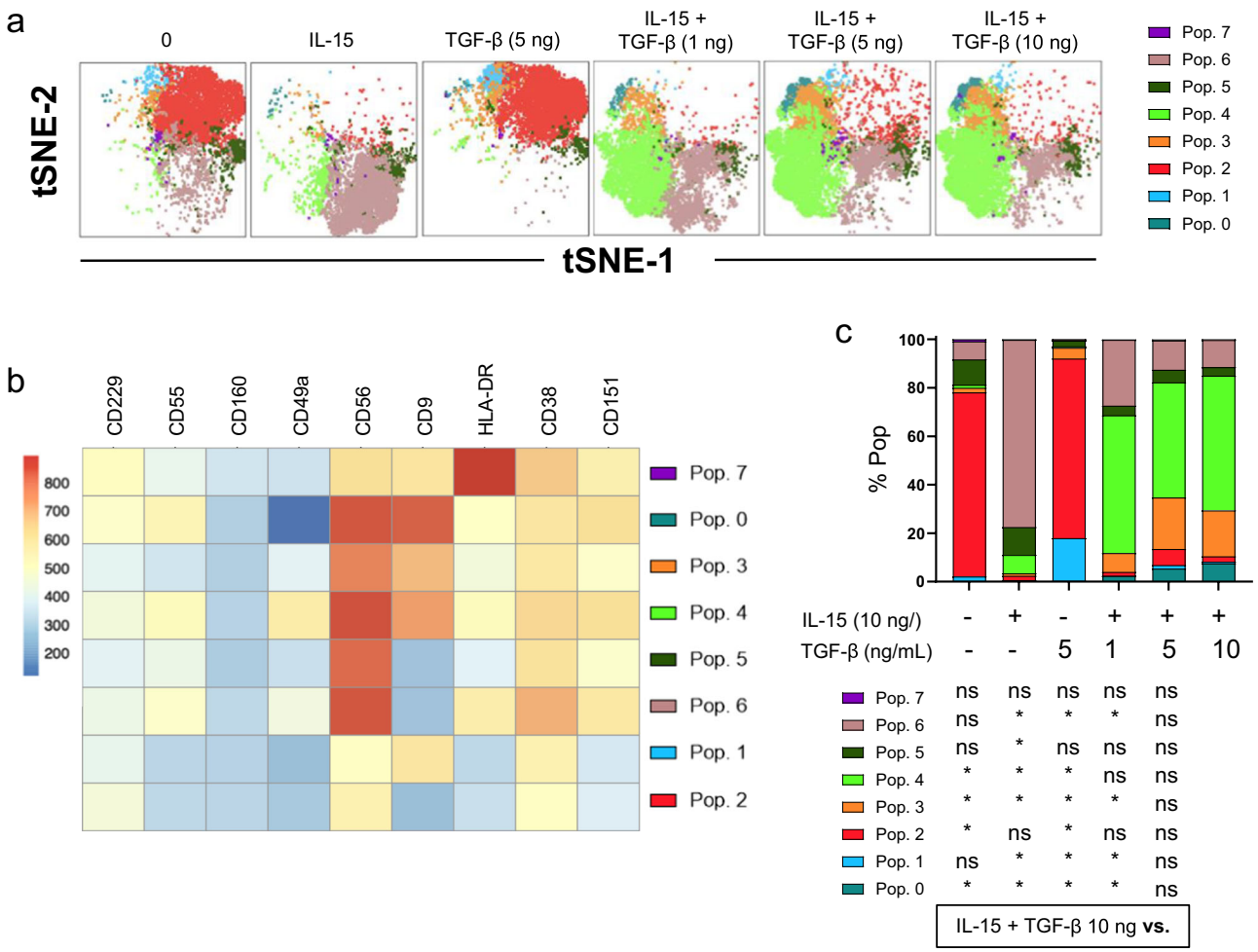

Fig. 7 | IL-15 and TGF-β induce an NK cell decidual-like phenotype. Unsupervised flow cytometric analysis using t-SNE and FlowSOM clustering tools to analyze the indicated markers (CD229, CD55, CD160, CD49a, CD56, CD9, HLA-DR, CD38, and CD151). NK cells were cultured with no cytokines, IL-15, 5 ng/mL TGF-β, IL-15 + 1 ng/mL TGF-β, IL-15 + 5 ng/mL TGF-β, IL-15 + 10 ng/mL TGF-β. IL-15 concentration was 10 ng/mL ($n = 7$). **a** t-SNE projection of NK cell populations (Pop) identified by the FlowSOM clustering tool for the specified markers. **b** Fluorescence intensity of each Pop as indicated in the column-scaled z-score. **c** Bars graph showing the percentage of each Pop at the six studied conditions. Significance of data was determined using the Wilcoxon matched-pairs signed-rank test by comparing each sample with the condition IL-15 + 10 ng/mL TGF-β. $^{*}p < 0.05$, $^{**}p < 0.01$ and ns no significant. Exact p values are provided in a file named Supplementary Data 2, under Fig. 7.

the CD9- NK cells, we found that Pop 5 and 6 were the most abundant when NK cells were cultured only in the presence of IL-15, and that the addition of TGF-β significantly decreased the frequency of these Pops. Furthermore, in several Pops, a TGF-β concentration-dependent effect was evident: Pops 0 and 3 increased with higher TGF-β concentration. Pop 7 is a very residual population (median of 0.53%) characterized by a very high expression of HLA-DR, which may suggest that these cells could be another ILC subset[54]. More studies are required to properly identify this very small subset. Altogether, these results suggest that IL-15 and TGF-β induce an activated and decidual-like phenotype on NK cells, which is characterized by higher expression of CD56, CD9, CD49a, CD151, CD55, CD38, and HLA-DR markers. We found these cells to be significantly expanded at S2, which correlates with very high levels of IL-15 and unchanged levels of TGF-β.

Discussion

In this work, we have studied the reconstitution of NK cells in pediatric patients with cancer who had undergone autoHSCT. We have analyzed NK cell subsets' phenotype, plasma levels of cytokines that are relevant in NK cell function, and we have performed in vitro experiments (scRNA-seq and flow cytometry) to explore the mechanisms behind the expansion of NK cells with a decidual-like phenotype during immune system reconstitution following autoHSCT. The cell surface phenotype and the transcriptome of NK cells vary considerably after autoHSCT[15–17] and, to the best of our knowledge, we have observed a previously undescribed change in NK cells phenotype towards a decidual-like and activated phenotype early after autoHSCT in pediatric patients. This activated and decidual-like phenotype is characterized by an increase of CD56, CD9, CD49a, CD151, CD38, HLA-DR, and CD55 expression shortly after autoHSCT. In addition, our in vitro experiments suggest that the combination of IL-15 and TGF-β induces, at least partially, this activated and decidual-like phenotype on NK cells.

It is known that TGF-β can induce the acquisition of a decidual-like phenotype in peripheral blood NK cells, characterized by the expression of CD9[55]. But in our study, we did not observe a significant change in TGF-β levels following autoHSCT (Fig. 5a). However, other authors have described that the combination of TGF-β with IL-15 induces the acquisition of decidual NK cell markers such as CD9, CD49a, and CD151[51,52,56]. Therefore, we hypothesized that the increased levels of IL-15 (Fig. 5a), together with TGF-β, may contribute to the acquisition of the NK cell decidual-like phenotype. In addition, other cytokines may have a role in the expansion of decidual-like NK cells early after autoHSCT, as for example GDF-15 and PlGF increased plasma levels (Fig. 5a). Importantly, we observed that GDF-15 levels associate with CD9 expression at S2 (Fig. 5b), suggesting that this cytokine could also have a role in the decidual-like phenotype acquisition. Nevertheless, more studies are needed in order to determine the effect of

GDF-15 and other cytokines, such as PlGF, on the expression of decidual markers such as CD9.

Several publications have shown an increased frequency of CD9+ circulating NK cells that associates with worse disease evolution[57–60] suggesting that CD9 expression on NK cells may be used as a biomarker in cancer patients, although we were not able to find an association between relapse and frequency of these cells. We speculate that the expansion of CD9+ NK cells is independent of the malignancy for which patients receive an autoHSCT, because we have previously published the same phenomenon in MM patients early after autoHSCT[17]. Evidently, we need larger and more homogeneous cohorts in order to establish CD9+ NK cells as a possible biomarker that may predict the evolution of cancer patients undergoing an autoHSCT in childhood.

In addition to the decidual NK cell markers, the cytokine milieu may also have a significant role in the observed changes in the expression of other markers early after autoHSCT. For example, correlation analyses (Fig. 5b) and in vitro experiments (Figs. 7 and S4) showed that the increased expression of CD56, activation markers (HLA-DR and CD38) and receptors such as CD26 and CD55, could be, at least in part, a consequence of the high IL-15 levels at S2 (Figs. 5b and S4), as it is shown in other studies[30,61–63]. However, TGF-β tended to counteract the effect of IL-15 (Figs. 7 and S4). Remarkably, analysis of data from both scRNA-seq (Fig. 6) and flow cytometry (Figs. 7 and S4) experiments suggests that the combination of IL-15 and TGF-β has a relevant role in the expansion of decidual-like NK cells early after autoHSCT, at least partially. The two in vitro experimental approaches showed that the combination of these two cytokines is responsible for the increased expression of CD9 (*CD9*), CD151 (*CD151*), and CD49a (*ITGA1*), markers that are typical of decidual NK cells[51,52,56]. Other markers that changed their expression at S2, such as CD26, CD160, and CD229, followed a similar trend of expression after the in vitro culture with IL-15 and TGF-β.

As expected, the frequencies of CD57+ NK cells in our pediatric patient cohort were lower than those observed in the cohort of MM adults[16]. This could be owed to the fact that cytomegalovirus infection, more prevalent in adults than in children, induces an expansion of CD57+ NK cells[64–66]. In addition, we have observed that NK cells express a more immature phenotype early after transplantation at S2 and acquire a more mature phenotype 180 days after autoHSCT, as shown by the increase of the mature NKG2A-CD57+ cell subset at S5. This is in agreement with the model of NK cell development and with the decreased NKG2A and increased CD57 expression during NK cell maturation[19,33]. These mature NKG2A−CD57+ NK cells exhibited a higher KIR expression, and they showed a tendency to expand after autoHSCT at S2 (Fig. 3d). These results are in line with reported data from adults receiving an alloHSCT[33]. Importantly, we have also described for the first time that in autoHSCT, NK cell education and maturation are uncoupled processes, since CD57 expression is not influenced by KIR expression, as it was previously described in alloHSCT[33,67].

The search and identification of prognostic biomarkers can be of great help to clinicians. We have observed a positive and significant correlation at S2 between the percentage of $CD56^{dim}$ NK cells and relapse (Fig. S2b), which express more CD57 than the $CD56^{bright}$ subset. These results are in agreement with data previously published by us and others in which low frequencies of circulating CD57+ and CD57+NKG2A− NK cells are associated with better clinical outcomes[16,68]. On the other hand, we have also observed that the increased expression levels of CD26 and CD55 at S2 seem to negatively associate with relapse (Fig. S2b). It is still unknown how these two receptors are involved in the evolution of autoHSCT and the underlying disease in pediatric patients. Some authors have found that high frequencies of transplanted CD26+ lymphocytes have a beneficial effect on NK cell recovery after autoHSCT in MM patients[69]. Conversely, others have shown that lower CD26 expression on different immune cell subtypes, including NK cells, of the donor stem cell harvest is associated with better survival in alloHSCT[70]. Regarding CD55, it has been described that, when expressed on NK cells, it makes them less effective at killing K562 targets[71]. Of note, it has been recently published that mouse NK cells present in the decidua were primarily the differentiated tissue resident NK cell subset, distinguished by their expression of CD55[72]. Definitely, it is required to explore if CD55 could be used as a human decidual (and decidual-like) NK cell marker. Nevertheless, these results have to be taken cautiously because our cohort is very small and heterogeneous. To validate these data, more studies, including a higher number of patients, are required.

Data availability

The data used to generate the main and Supplementary Figures are provided in a file named Supplementary Data 1, with each figure's data presented in a separate Excel tab (Figs. 1–7 and S2–S4). Exact *p* values are provided in Supplementary Data 2, also organized by figure in separate tabs (Figs. 1–7 and S2–S4). The scRNA-seq data have been deposited in the Gene Expression Omnibus (GEO) under accession number GSE255347. In accordance with ethical approvals and participant consents, access to raw data is restricted to approved research projects. All other data are available from the corresponding author upon reasonable request.

Received: 3 April 2024; Accepted: 13 May 2025;
Published online: 28 May 2025

References

1. Pinto, N. R. et al. Advances in risk classification and treatment strategies for neuroblastoma. *J. Clin. Oncol.* **33**, 3008–3017 (2015).
2. Saleh, K., Michot, J.-M., Camara-Clayette, V., Vassetsky, Y. & Ribrag, V. Burkitt and Burkitt-like lymphomas: a systematic review. *Curr. Oncol. Rep.* **22**, 33 (2020).
3. Passweg, J. R. et al. The EBMT activity survey on hematopoietic-cell transplantation and cellular therapy 2018: CAR-T's come into focus. *Bone Marrow Transpl.* **55**, 1604–1613 (2020).
4. Porrata, L. F., Ingle, J. N., Litzow, M. R., Geyer, S. & Markovic, S. N. Prolonged survival associated with early lymphocyte recovery after autologous hematopoietic stem cell transplantation for patients with metastatic breast cancer. *Bone Marrow Transpl.* **28**, 865–871 (2001).
5. Porrata, L. F. et al. Early lymphocyte recovery predicts superior survival after autologous hematopoietic stem cell transplantation in multiple myeloma or non-Hodgkin lymphoma. *Blood* **98**, 579–585 (2001).
6. Porrata, L. F. et al. Early lymphocyte recovery post-autologous haematopoietic stem cell transplantation is associated with better survival in Hodgkin's disease. *Br. J. Haematol.* **117**, 629–633 (2002).
7. Porrata, L. F. et al. Early lymphocyte recovery predicts superior survival after autologous stem cell transplantation in non-Hodgkin lymphoma: a prospective study. *Biol. Blood Marrow Transplant.* **14**, 807–816 (2008).
8. Porrata, L. F. Natural killer cells are key host immune effector cells affecting survival in autologous peripheral blood hematopoietic stem cell transplantation. *Cells* **11**, 3469 (2022).
9. Prager, I. & Watzl, C. Mechanisms of natural killer cell-mediated cellular cytotoxicity. *J. Leukoc. Biol.* **105**, 1319–1329 (2019).
10. Caligiuri, M. A. Human natural killer cells. *Blood* **112**, 461–469 (2008).
11. Freud, A. G., Mundy-Bosse, B. L., Yu, J. & Caligiuri, M. A. The broad spectrum of human natural killer cell diversity. *Immunity* **47**, 820–833 (2017).
12. Long, E. O., Sik Kim, H., Liu, D., Peterson, M. E. & Rajagopalan, S. Controlling natural killer cell responses: integration of signals for activation and inhibition. *Annu. Rev. Immunol.* **31**, 227–258 (2013).
13. Vivier, E., Ugolini, S., Blaise, D., Chabannon, C. & Brossay, L. Targeting natural killer cells and natural killer T cells in cancer. *Nat. Rev. Immunol.* **12**, 239–252 (2012).
14. Cerwenka, A. & Lanier, L. L. Natural killer cell memory in infection, inflammation and cancer. *Nat. Rev. Immunol.* **16**, 112–123 (2016).
15. Jacobs, B. et al. NK cell subgroups, phenotype, and functions after autologous stem cell transplantation. *Front. Immunol.* **6**, 583 (2015).

16. Orrantia, A. et al. NK cell reconstitution after autologous hematopoietic stem cell transplantation: association between NK cell maturation stage and outcome in multiple myeloma. *Front. Immunol.* **12**, 748207 (2021).
17. Orrantia, A. et al. In vivo expansion of a CD9+ decidual-like NK cell subset following autologous hematopoietic stem cell transplantation. *iScience* **25**, 105235 (2022).
18. Cursons, J. et al. A gene signature predicting natural killer cell infiltration and improved survival in melanoma patients. *Cancer Immunol. Res.* **7**, 1162–1174 (2019).
19. Orrantia, A., Terrén, I., Astarloa-Pando, G., Zenarruzabeitia, O. & Borrego, F. Human NK cells in autologous hematopoietic stem cell transplantation for cancer treatment. *Cancers***13**, 1589 (2021).
20. Arteche-López, A. et al. Multiple myeloma patients in long-term complete response after autologous stem cell transplantation express a particular immune signature with potential prognostic implication. *Bone Marrow Transpl.* **52**, 832–838 (2017).
21. Marra, J. et al. KIR and HLA genotypes predictive of low-affinity interactions are associated with lower relapse in autologous hematopoietic cell transplantation for acute myeloid leukemia. *J. Immunol.* **194**, 4222–4230 (2015).
22. Venstrom, J. M. et al. KIR and HLA genotypes are associated with disease progression and survival following autologous hematopoietic stem cell transplantation for high-risk neuroblastoma. *Clin. Cancer Res.* **15**, 7330–7334 (2009).
23. Leung, W. et al. Inhibitory KIR-HLA receptor-ligand mismatch in autologous haematopoietic stem cell transplantation for solid tumour and lymphoma. *Br. J. Cancer* **97**, 539–542 (2007).
24. Stringaris, K. & Barrett, A. J. The importance of natural killer cell killer immunoglobulin-like receptor-mismatch in transplant outcomes. *Curr. Opin. Hematol.* **24**, 489–495 (2017).
25. Gabriel, I. H. et al. Interaction between KIR3DS1 and HLA-Bw4 predicts for progression-free survival after autologous stem cell transplantation in patients with multiple myeloma. *Blood* **116**, 2033–2039 (2010).
26. Erbe, A. K. et al. Neuroblastoma patients' KIR and KIR-ligand genotypes influence clinical outcome for dinutuximab-based immunotherapy: a report from the Children's Oncology Group. *Clin. Cancer Res.* **24**, 189–196 (2018).
27. Orrantia, A. et al. A NKp80-based identification strategy reveals that CD56neg NK cells are not completely dysfunctional in health and disease. *iScience* **23**, 101298 (2020).
28. Deaglio, S. et al. Human CD38 and CD16 are functionally dependent and physically associated in natural killer cells. *Blood* **99**, 2490–2498 (2002).
29. Erokhina, S. A. et al. HLA-DR+ NK cells are mostly characterized by less mature phenotype and high functional activity. *Immunol. Cell Biol.* **96**, 212–228 (2018).
30. Yamabe, T. et al. Induction of the 2B9 antigen/dipeptidyl peptidase IV/CD26 on human natural killer cells by IL-2, IL-12 or IL-15. *Immunology* **91**, 151–158 (1997).
31. McKinney, E. F. et al. A CD8+ NK cell transcriptomic signature associated with clinical outcome in relapsing remitting multiple sclerosis. *Nat. Commun.* **12**, 635 (2021).
32. Solomon, K. R., Chan, M. & Finberg, R. W. Expression of GPI-anchored complement regulatory proteins CD55 and CD59 differentiates two subpopulations of human CD56+CD3- lymphocytes (NK cells). *Cell Immunol.* **165**, 294–301 (1995).
33. Björkström, N. K. et al. Expression patterns of NKG2A, KIR, and CD57 define a process of CD56 dim NK-cell differentiation uncoupled from NK-cell education. *Blood* **116**, 3853–3864 (2010).
34. Vento-Tormo, R. et al. Single-cell reconstruction of the early maternal–fetal interface in humans. *Nature* **563**, 347–353 (2018).
35. Koopman, L. A. et al. Human decidual natural killer cells are a unique NK cell subset with immunomodulatory potential. *J. Exp. Med.* **198**, 1201–1212 (2003).
36. Li, H. et al. CD49a regulates the function of human decidual natural killer cells. *Am. J. Reprod. Immunol.* **81**, 1–8 (2019).
37. Farley, M. J., Bartlett, D. B., Skinner, T. L., Schaumberg, M. I. A. A. & Jenkins, D. G. Immunomodulatory function of interleukin-15 and its role in exercise, immunotherapy, and cancer outcomes. *Med. Sci. Sports Exerc.* **55**, 558–568 (2023).
38. Huntington, N. D. et al. IL-15 trans-presentation promotes human NK cell development and differentiation in vivo. *J. Exp. Med.* **206**, 25–34 (2009).
39. Carson, W. E. et al. Interleukin (IL) 15 is a novel cytokine that activates human natural killer cells via components of the IL-2 receptor. *J. Exp. Med.* **180**, 1395–1403 (1994).
40. Porrata, L. F. et al. Interleukin-15 affects patient survival through natural killer cell recovery after autologous hematopoietic stem cell transplantation for non-Hodgkin lymphomas. *Clin. Dev. Immunol.* **2010**, 914945 (2010).
41. Bottino, C. et al. Natural killer cells and neuroblastoma: tumor recognition, escape mechanisms, and possible novel immunotherapeutic approaches. *Front. Immunol.* **5**, 56 (2014).
42. Zaiatz-Bittencourt, V., Finlay, D. K. & Gardiner, C. M. Canonical TGF-β signaling pathway represses human NK cell metabolism. *J. Immunol.* **200**, 3934–3941 (2018).
43. Rautela, J. et al. Therapeutic blockade of activin-A improves NK cell function and antitumor immunity. *Sci. Signal.* **12**, https://doi.org/10.1126/scisignal.aat7527 (2019).
44. Castriconi, R. et al. Neuroblastoma-derived TGF-β1 modulates the chemokine receptor repertoire of human resting NK cells. *J. Immunol.* **190**, 5321–5328 (2013).
45. Zenarruzabeitia, O., Vitallé, J., Astigarraga, I. & Borrego, F. Natural killer cells to the attack: combination therapy against neuroblastoma. *Clin. Cancer Res.* **23**, 615–617 (2017).
46. Kleinertz, H. et al. Circulating growth/differentiation factor 15 is associated with human CD56bright natural killer cell dysfunction and nosocomial infection in severe systemic inflammation. *EBioMedicine* **43**, 380–391 (2019).
47. Albonici, L., Giganti, M. G., Modesti, A., Manzari, V. & Bei, R. Multifaceted role of the Placental Growth Factor (PlGF) in the antitumor immune response and cancer progression. *Int. J. Mol. Sci.* **20**, 2970 (2019).
48. Fredriksson, L., Li, H. & Eriksson, U. The PDGF family: four gene products form five dimeric isoforms. *Cytokine Growth Factor Rev.* **15**, 197–204 (2004).
49. Lokker, N. A., Sullivan, C. M., Hollenbach, S. J., Israel, M. A. & Giese, N. A. Platelet-derived growth factor (PDGF) autocrine signaling regulates survival and mitogenic pathways in glioblastoma cells: evidence that the novel PDGF-C and PDGF-D ligands may play a role in the development of brain tumors. *Cancer Res.* **62**, 3729–3735 (2002).
50. Ma, S. et al. PDGF-D-PDGFRβ signaling enhances IL-15–mediated human natural killer cell survival. *Proc. Natl. Acad. Sci. USA* **119**, e2114134119 (2022).
51. Hawke, L. G., Mitchell, B. Z. & Ormiston, M. L. TGF-β and IL-15 Synergize through MAPK pathways to drive the conversion of human NK cells to an innate lymphoid Cell 1-like phenotype. *J. Immunol.* **204**, 3171–3181 (2020).
52. Du, X. et al. Human-induced CD49a+ NK cells promote fetal growth. *Front. Immunol.* **13**, 821542 (2022).
53. Crinier, A. et al. High-dimensional single-cell analysis identifies organ-specific signatures and conserved NK cell subsets in humans and mice. *Immunity* **49**, 971–986.e5 (2018).
54. Cruz-Zárate, D. et al. Innate lymphoid cells have decreased HLA-DR expression but retain their responsiveness to TLR ligands during sepsis. *J. Immunol.* **201**, 3401–3410 (2018).
55. Keskin, D. B. et al. TGFβ promotes conversion of CD16+ peripheral blood NK cells into CD16- NK cells with similarities to decidual NK cells. *Proc. Natl. Acad. Sci. USA* **104**, 3378–3383 (2007).

56. Siewiera, J. et al. Natural cytotoxicity receptor splice variants orchestrate the distinct functions of human natural killer cell subtypes. *Nat. Commun.* **6**, 10183 (2015).
57. Albini, A. & Noonan, D. M. Decidual-like NK cell polarization: from cancer killing to cancer nurturing. *Cancer Discov.* **11**, 28–33 (2021).
58. Gallazzi, M. et al. Prostate cancer peripheral blood NK cells show enhanced CD9, CD49a, CXCR4, CXCL8, MMP-9 production and secrete monocyte-recruiting and polarizing factors. *Front. Immunol.* **11**, 586126 (2021).
59. Bruno, A. et al. Angiogenin and the MMP9-TIMP2 axis are up-regulated in proangiogenic, decidual NK-like cells from patients with colorectal cancer. *FASEB J.* **32**, 5365–5377 (2018).
60. Gonzalez, V. D. et al. High-grade serous ovarian tumor cells modulate NK cell function to create an immune-tolerant microenvironment. *Cell Rep.* **36**, 109632 (2021).
61. Boyiadzis, M. et al. Up-regulation of NK cell activating receptors following allogeneic hematopoietic stem cell transplantation under a lymphodepleting reduced intensity regimen is associated with elevated IL-15 levels. *Biol. Blood Marrow Transplant.* **14**, 290–300 (2008).
62. Erokhina, S. A. et al. HLA-DR-expressing NK cells: effective killers suspected for antigen presentation. *J. Leukoc. Biol.* **109**, 327–337 (2021).
63. Wang, L., Halliday, D., Johnson, P. M. & Christmas, S. E. Expression of complement regulatory proteins on human natural killer cell subsets. *Immunol. Lett.* **112**, 104–109 (2007).
64. Lam, J. K. P. et al. Co-infection of cytomegalovirus and epstein-barr virus diminishes the frequency of CD56dimNKG2A+KIR− NK cells and contributes to suboptimal control of EBV in immunosuppressed children with post-transplant lymphoproliferative disorder. *Front. Immunol.* **11**, 1–12 (2020).
65. Lopez-Sejas, N. et al. Effect of CMV and aging on the differential expression of CD300a, CD161, T-bet, and eomes on NK cell subsets. *Front. Immunol.* **7**, 476 (2016).
66. Campos, C. et al. Effect of age and CMV on NK cell subpopulations. *Exp. Gerontol.* **54**, 130–137 (2014).
67. Pradier, A. et al. Modulation of T-bet and eomes during maturation of peripheral blood NK cells does not depend on licensing/educating KIR. *Front. Immunol.* **7**, 299 (2016).
68. Muntasell, A. et al. High numbers of circulating CD57+ NK cells associate with resistance to hER2-specific therapeutic antibodies in HER2+ primary breast cancer. *Cancer Immunol. Res.* **7**, 1280–1292 (2019).
69. Kopinska, A. et al. The importance of the number of transplanted cells with dipeptidyl peptidase-4 expression on the haematopoietic recovery and lymphocyte reconstitution in patients with multiple myeloma after autologous haematopoietic stem-cell transplantation. *Hematol. Oncol.* **35**, 225–231 (2017).
70. Kandekar, S. et al. Low levels of CD26 on certain cellular subtypes of donor harvest is associated with better clinical outcomes post allogeneic stem cell transplantation through regulation of NF-κB pathway and pro-inflammatory cytokines. *Int. Immunopharmacol.* **125**, 111054 (2023).
71. Finberg, R. W., White, W. & Nicholson-Weller, A. Decay-accelerating factor expression on either effector or target cells inhibits cytotoxicity by human natural killer cells. *J. Immunol.* **149**, 2055–2060 (1992).
72. Han, M. et al. IL-21R-STAT3 signalling initiates a differentiation program in uterine tissue-resident NK cells to support pregnancy. *Nat. Commun.* **14**, 7109 (2023).

Acknowledgements

We thank all patients and families who participated in this study, the staff from the Basque Biobank for Research, and the staff from the Flow Cytometry and Genetics-Genomics Platforms of Biobizkaia Health Research Institute. We also thank Iñigo Terrén and Rafael González for their critical reading of the manuscript. This work was funded by the following grants: Fundación AECC-Spanish Association Against Cancer (PROYE16074BORR) and BIOEF (Basque Foundation for Research and Innovation)-EiTB Maratoia (BIO20/CI/009). G.A.-P. and A.A.-I. are recipients of a predoctoral contract funded by Fundación AECC-Spanish Association Against Cancer (PRDVZ21440ASTA and PRDVZ234209AMAR). D.P.-A. and A.T. are recipients of a fellowship from the Fundación AECC-Spanish Association Against Cancer (PPLAB212164POLA and PPLAB223829TIJE). A.L.-P. is recipient of a predoctoral contract funded by La Caixa Foundation (100010434; LCF/BQ/DI22/11940012). G.A.-P. and A.A.-I. are recipients of a fellowship from the Jesús de Gangoiti Barrera Foundation (FJGB21/001 and FJBG21/005). B.M.-M. is recipient of a post-doctoral contract funded by CSYF, European Social Fund, Andalucía, Spain (RH-0060-2020). A.S. is recipient of a grant from the Margarita Salas program, for the requalification of the Spanish university system 2021-2023, financed by the European Union—Next Generation EU. L.A. is an Ikerbasque Research Fellow (COFUND program H2020-MSCA-COFUND-2020-101034228-WOLFRAM2) and F.B. is an Ikerbasque Research Professor, Ikerbasque, Basque Foundation for Science.

Author contributions

F.B., G.A.-P., and O.Z. conceived the project; F.B., G.A.-P., and A.O. designed the experiments; G.A.-P., D.P.-A., V.S., A.T., M.R., R.P.-G., and L.A. performed experiments; G.A.-P., D.P.-A., S.P.-F., N.G.B., A.Z.-G., and A.T. conducted data analysis; J.J.U. and I.A. obtained the clinical samples and clinical data from patients; B.M.-M. analyzed HLA and KIR haplotypes; G.A.-P., L.A., V.S., N.G.B., and F.B. designed figures; A.O., A.A.-I., A.S., V.S., A.L.-P., and O.Z. provided intellectual input; G.A.-P., F.B. N.G.B., and L.A. wrote the manuscript; all authors critically reviewed the manuscript.

Competing interests

The authors declare no competing interests.

Additional information

Supplementary information The online version contains supplementary material available at https://doi.org/10.1038/s43856-025-00911-w.

Correspondence and requests for materials should be addressed to Francisco Borrego.

Peer review information *Communications Medicine* thanks the anonymous reviewers for their contribution to the peer review of this work. [A peer review file is available].

Gabirel Astarloa-Pando[1], Diego Polanco-Alonso[1], Víctor Sandá[1], Ane Orrantia[1], Ainhoa Amarilla-Irusta[1], Silvia Pérez-Fernández[2], Raquel Pérez-Garay[1,3], Arrate Sevilla[1,4], Ainara Lopez-Pardo[1], Aritz Tijero[1], José J. Úriz[5], Mercedes Rey[6], Itziar Astigarraga[7,8], Bárbara Manzanares-Martin[9], Aitor Zarandona-Garai[2], Naiara G. Bediaga[2], Laura Amo[1,10], Olatz Zenarruzabeitia[1,4] & Francisco Borrego[1,10]

[1]Immunopathology Group, Biobizkaia Health Research Institute, Barakaldo, Spain. [2]Bioinformatics, Biostatistics and Information Systems Platform, Biobizkaia Health Research Institute, Barakaldo, Spain. [3]Clinical Analysis Service, Cruces University Hospital, Barakaldo, Spain. [4]Department of Genetics, Physical Anthropology and Animal Physiology, Faculty of Science and Technology, University of the Basque Country (UPV/EHU), Leioa, Spain. [5]Biogipuzkoa Health Research Institute, Service of Pediatrics, Donostia University Hospital, Donostia-San Sebastián, Spain. [6]Biogipuzkoa Health Research Institute, Service of Immunology, Donostia University Hospital, Donostia-San Sebastián, Spain. [7]Pediatric Oncology Group, Department of Pediatrics, Biobizkaia Health Research Institute, Cruces University Hospital, Barakaldo, Spain. [8]Department of Pediatrics, Faculty of Medicine and Nursing, University of the Basque Country (UPV/EHU), Leioa, Spain. [9]Maimónides Biomedical Research Institute of Córdoba (IMIBIC), Immunology and Allergy Department of Reina Sofía University Hospital and Transfusion, Tissue and Cells Centre (CTTC), Córdoba, Spain. [10]Ikerbasque, Basque Foundation for Science, Bilbao, Spain. e-mail: francisco.borregorabasco@bio-bizkaia.eus